Metastasis of cholangiocarcinoma is promoted by extended high-mannose glycans

Diane Dayoung Park[a,1,2], Chatchai Phoomak[b,3], Gege Xu[a], Laura P. Olney[c], Khiem A. Tran[c], Simon S. Park[d], Nathan E. Haigh[c], Guillaume Luxardi[c], Worachart Lert-itthiporn[b], Michiko Shimoda[c], Qiongyu Li[a], Nobuyuki Matoba[e], Fernando Fierro[f], Sopit Wongkham[b], Emanual Maverakis[c], and Carlito B. Lebrilla[a]

[a]Department of Chemistry, University of California, Davis, CA 95616; [b]Department of Biochemistry, Faculty of Medicine, Khon Kaen University, 40002 Khon Kaen, Thailand; [c]Department of Dermatology, University of California Davis School of Medicine, Sacramento, CA 95817; [d]Department of Surgery, Beth Israel Deaconess Medical Center, Harvard Medical School, Boston, MA 02215; [e]Department of Pharmacology and Toxicology, University of Louisville School of Medicine, Louisville, KY 40202; and [f]Department of Cell Biology and Human Anatomy, University of California Davis School of Medicine, Sacramento, CA 95817

Edited by Chi-Huey Wong, Scripps Research, Taipei, Taiwan, and approved February 28, 2020 (received for review September 23, 2019)

Membrane-bound oligosaccharides form the interfacial boundary between the cell and its environment, mediating processes such as adhesion and signaling. These structures can undergo dynamic changes in composition and expression based on cell type, external stimuli, and genetic factors. Glycosylation, therefore, is a promising target of therapeutic interventions for presently incurable forms of advanced cancer. Here, we show that cholangiocarcinoma metastasis is characterized by down-regulation of the Golgi α-mannosidase I coding gene *MAN1A1*, leading to elevation of extended high-mannose glycans with terminating α-1,2-mannose residues. Subsequent reshaping of the glycome by inhibiting α-mannosidase I resulted in significantly higher migratory and invasive capabilities while masking cell surface mannosylation suppressed metastasis-related phenotypes. Exclusive elucidation of differentially expressed membrane glycoproteins and molecular modeling suggested that extended high-mannose glycosylation at the helical domain of transferrin receptor protein 1 promotes conformational changes that improve noncovalent interaction energies and lead to enhancement of cell migration in metastatic cholangiocarcinoma. The results provide support that α-1,2-mannosylated *N*-glycans present on cancer cell membrane proteins may serve as therapeutic targets for preventing metastasis.

metastasis | cholangiocarcinoma | mass spectrometry | glycosylation | membrane proteins

The lethality of cancer generally lies in the event that metastatic tumors detach from the primary site and colonize distant tissues. Although the mechanisms of tissue invasion and migration into and out of the vasculature have been described in detail (1–3), preventive therapy remains sparse. Cholangiocarcinoma (CCA) is a rare form of highly metastatic cancer that has a poor prognosis and rising incidence (4). Currently, surgical removal is the only curative treatment albeit under high risk of postsurgical complications. However, diagnostic symptoms are often not evident until advanced stages. The limited number of treatment options is confounded by a lack in understanding of how CCA cells acquire the capabilities to metastasize. Molecular-level details are thus needed of the underlying causes of the metastatic cascade prior to spread and formation of secondary tumors, which often precludes surgical interventions and radiotherapies.

Considerable evidence demonstrates that glycosylation is closely correlated with malignancy (5–10). Compared to healthy controls, tumor cells showed marked changes in glycan expression as a result of the dysregulation of glycosyltransferases, producing increases in β-1,6 branching, α-2,6-sialylation, sialyl Lewis X determinants, Tn epitopes, and/or T antigens (11–16). Certain glycosylation changes appear to depend on cancer cell origin. For example, samples derived from patients with prostate and breast cancer specifically overexpressed fucosylated and high-mannose type glycans, respectively (17–19). Such disease-specific changes may be involved in modulating tumor aggressiveness.

Metastatic transformation of cancer cells is often accompanied by phenotypic diversity. Spread by means of the venous system requires both adhesive capability and evasion of immune surveillance. Once they survive in the circulation, cells that have arrested at a secondary site must be able to initiate growth, maintain viability, reshape their cytoskeletal architecture, and migrate through the basement membrane, processes that are regulated by molecular interactions with the new environment (20). Thus, bioconjugates positioned on the surface of tumor cells can provide key insight into metastatic outcome. In particular, membrane-associated glycoconjugates have been shown to play a distinct role in mediating contact with surrounding substances and dictating the rigidity of the underlying scaffold (21–25). Alteration of glycosylation during metastatic transformation may confer a functional advantage,

Significance

Cells assemble a dense layer composed of glycans on the plasma membrane, following nontemplated processes that can be perturbed during malignancy. The intrinsic heterogeneity of glycosylation presents challenges to unambiguously identifying disease-specific transformations and selectively targeting them while preventing off-target events. Here, we show that extended high-mannose glycans are more abundantly expressed in metastatic cholangiocarcinoma than in the parental tumor cells from which they were derived. With structure-guided manipulations, extended high-mannose glycans were implicated in supporting cholangiocarcinoma metastasis by enhancing the ability to translocate, invade surrounding basement membrane matrix, and migrate through micropores. Isolation of high-mannose–bearing glycoproteins and computational modeling suggested that dominance of extended high-mannose glycosylation drives metastatic progression by indirectly strengthening extracellular protein complexes.

Author contributions: D.D.P., C.P., and C.B.L. designed research; D.D.P., C.P., G.X., L.P.O., K.A.T., S.S.P., N.E.H., G.L., and Q.L. performed research; C.P., K.A.T., S.S.P., M.S., N.M., F.F., S.W., and E.M. contributed new reagents/analytic tools; D.D.P., G.X., L.P.O., N.E.H., G.L., and W.L.-i. analyzed data; and D.D.P. and C.B.L. wrote the paper.

The authors declare no competing interest.

This article is a PNAS Direct Submission.

[1]Present address: Department of Surgery, Beth Israel Deaconess Medical Center, Harvard Medical School, Boston, MA 02215.

[2]To whom correspondence may be addressed. Email: dpark4@bidmc.harvard.edu.

[3]Present address: Department of Therapeutic Radiology, Yale School of Medicine, New Haven, CT 06510.

This article contains supporting information online at https://www.pnas.org/lookup/suppl/doi:10.1073/pnas.1916498117/-/DCSupplemental.

First published March 25, 2020.

accounting for the ability of cells to invade and grow in distant organs. However, the biological importance of glycan structures in relation to metastatic progression remains unclear. To demonstrate their significance, support for the glycosylation changes that persist in metastasis is still needed.

Targeted therapy relies on the ability to unambiguously identify distinguishing features of malignant transformations. Here, we investigated whether membrane-associated glycans serve as markers in differentiating highly metastatic CCA from parental tumor cells and whether such changes in glycosylation are involved in molecular processes that promote metastatic spread. Our results provide evidence that the presentation of α-1,2-mannose–containing *N*-glycan structures on cell surface proteins in high abundance enhances CCA migration and invasion. Deexposing extracellular mannosylation compromised the migratory and invasion capabilities of metastatic CCA in vitro and overexpression of Golgi α-1,2-mannosidase IA reduced tumor growth in vivo, proposing α-1,2-mannosylation as among promising targets for inhibiting the progression of CCA metastasis.

Results

Increases in Extended High-Mannose Glycans Are Metastasis-Specific Transformations. To establish a highly metastatic CCA subpopulation, cells that formed lung metastasis were isolated after five successive i.v. passages into NOD/*scid*/Jak3^{null} (NOJ) mice (26). This protocol was performed with two types of intrahepatic CCA with different aggressive scales (Fig. 1*A*). We found prominent differences in growth properties as well as in metastasis-related phenotypes including proliferation, migration, and invasion between parental CCA cells (KKU-213A and KKU-213B) and their respective metastatic subclones (KKU-213AL5 and KKU-213BL5) in vitro and in vivo (27). In addition, metastatic CCA cells exhibited enhanced range of locomotion in comparison to parental cells (Fig. 1*B* and Movies S1 and S2).

For initial comparative studies between parental and metastatic cells, we purified and analyzed *N*-glycans from cell surface glycoproteins by nanoflow liquid chromatography-tandem mass spectrometry (LC-MS/MS) to inspect structural changes that accompany metastasis. This approach revealed that the composition of glycans on metastatic cells was not sufficiently distinct from that on parental cells. Rather, their expression levels were differentially regulated. To evaluate macrolevel changes, glycans expressed in parental and metastatic CCA cells were grouped based on their features (Fig. 1*C*). High-mannose glycans exhibited one of the most prominent differences among all comparisons ($P < 0.05$). Within the high-mannose subtype, extended structures (>Man 6) were distinguished from shorter structures (<Man 6) not only by their size but also by their terminating linkage positions (Fig. 1*D*). Whereas Man 7, Man 8, and Man 9 terminate with one or more α-1,2-mannosyl units, Man 5 possesses terminal α-1,3- and α-1,6-mannosyl units. The abundances of structures that corresponded to Man 7, Man 8, and Man 9 consistently trended upward in highly metastatic CCA cells compared to parental cells (Fig. 1*E*).

Given that glycan changes can arise from aberrant expression of the glycosyltransferase and glycosidase enzymes involved in the biosynthetic pathway, we assessed the expression of genes involved in *N*-glycosylation in parental and metastatic CCA cells by qRT-PCR. Among the gene family related to mannose processing, changes in expression of the α-1,2-mannosidase–coding genes *MAN1A1* and *MAN1B1* exceeded the threshold value (Fig. 1*F*). In particular, *MAN1A1* expression was significantly lower in both metastatic CCA cells compared to their corresponding parental cells, up to 5.9-fold in KKU-213AL5 ($P < 0.001$) and 6.6-fold in KKU-213BL5 ($P < 0.001$). Flow cytometry confirmed that MAN1A1 expression at the protein level was also reduced in metastatic CCA cells (Fig. 1*G*). Together, these data delineate a potential role of extended high-mannose glycan structures that overoccupy the cell surface upon metastatic transformation.

Enhancing High-Mannose Glycan Production Increases Metastatic Potential of Cancer Cells. On the premise that glycan expression is unique during metastasis, we specifically evaluated the participation of extended high-mannose structures in regulating metastatic behavior. We first assessed whether inducing increases in high-mannose glycans facilitates the progression of CCA into metastatic cells. With mass spectrometric analysis, we showed previously that cell surfaces can be remodeled to favor production of extended high-mannose glycans to varying degrees via inhibition of the α-mannosidase I enzyme by kifunensine (28, 29). Similarly, CCA cells with maximal levels of extended high-mannose glycan expression and minimal amounts of shorter high-mannose glycans were generated following a dose–response screening (*SI Appendix*, Fig. S1). To probe nonlateral migration, we followed the number of cells that passed through micropores and observed that kifunensine-treated KKU-213A and KKU-213B cells exhibited up to 1.9-fold ($P < 0.05$) greater migratory capabilities in comparison to untreated cells (Fig. 2 *A* and *B*). In addition to assessing cell migration, when the invasiveness of treated cells was examined using a Matrigel-coated Boyden chamber assay, cell invasion through the basement membrane matrix was accentuated up to 1.6-fold ($P < 0.05$) (Fig. 2*C*). Varying the treatment conditions resulted in concentration-dependent increases in migratory and invasive capabilities in both KKU-213A and KKU-213B cells, suggesting a possible mechanism that relies on the amount of high-mannose glycan expression.

In addition to transmigration, we assessed differences in lateral migration between untreated and kifunensine-treated parental CCA cells. Because wound sizes vary, relative percentage of closure was used to compare the migratory distance covered by treated cells relative to untreated cells (Fig. 2*D*). At the concentration that produced maximal high-mannose glycan expression, the mean migratory velocity of treated KKU-213A and KKU-213B cells was ∼34% and 19% higher than that of untreated cells, respectively (Fig. 2*E*). The lateral migratory distance covered by treated KKU-213A cells within 24 h was such that the scratch wound was nearly closed. To test for the generality of these findings, we measured the effects of kifunensine-induced overproduction of high-mannose glycans in other cancer types and found that they exhibited similar migratory and invasive advantages over untreated controls (*SI Appendix*, Figs. S2 and S3). These results provided support that elevated abundances of extended high-mannose glycan structures on cell membrane proteins enhance the metastatic potential of CCA cells.

Masking Extracellular High-Mannose Glycans Reduces Metastatic Phenotypes. After demonstrating that increasing high-mannose glycan expression contributes to metastatic behaviors, we sought to investigate whether blocking these structures diminishes metastasis. Metastatic KKU-213AL5 and KKU-213BL5 cells were challenged with Concanavalin A (ConA), a cell-impermeable mannose-specific legume seed lectin that binds with high specificity to terminal α-mannose residues, and examined for changes in metastatic-related phenotypes. To ensure that formation of cell aggregates did not impede the observed behaviors, cells were examined under a range of incubation conditions (*SI Appendix*, Fig. S4). In measuring the wound healing response, we found that uncapped KKU-213AL5 and KKU-213BL5 cells closed a greater proportion of the scratch wound within 24 h compared to ConA-capped cells by a factor of 2.0 ($P < 0.01$) and 2.4 ($P < 0.01$), respectively (Fig. 3 *A* and *B*). Relatedly, a reduction of up to 4.7-fold ($P < 0.001$) was observed in the number of metastatic CCA cells that migrated nonlaterally through microporous polycarbonate membranes when high-mannose glycans were capped with ConA (Fig. 3*C*). The number of ConA-capped metastatic CCA cells that invaded and migrated through membranes coated with basement

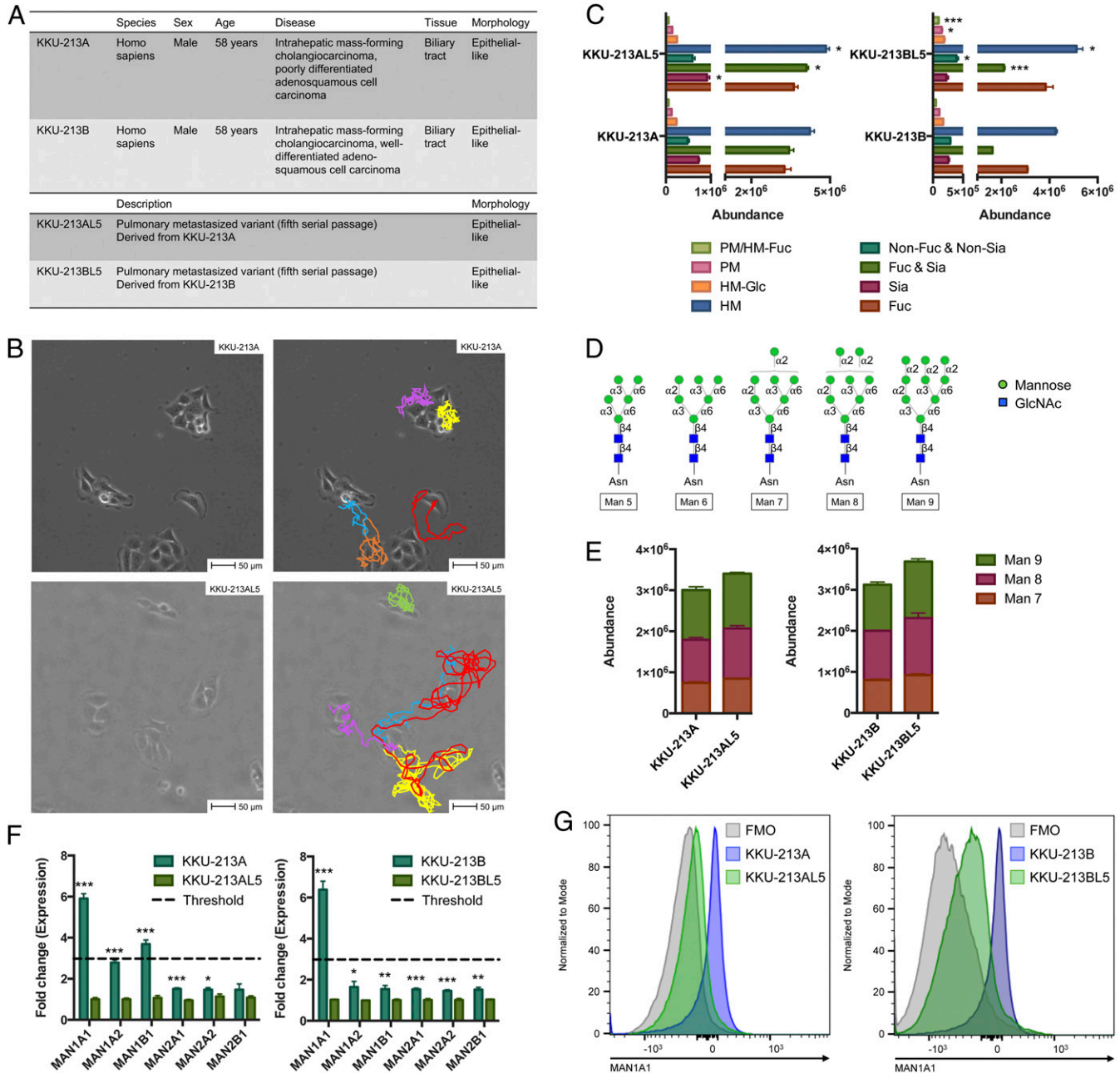

Fig. 1. Analysis of parental and metastatic CCA cell surface glycosylation. (*A*) Morphological and phenotypic characterization of CCA cells. (*B*) Image capture of live cell microscopy videos of KKU-213A and KKU-213AL5 growth at the beginning of a 24-h incubation at 37 °C. Per given cell, displacement was tracked frame by frame. Colored lines (*Right*) indicate the direction and extent of each cell's movement. (Scale bars, 50 μm.) (*C*) Quantitative changes in *N*-glycan abundances between parental and metastatic CCA cells based on their compositional features. Groups include high mannose (HM), paucimannose (PM), fucosylated (Fuc), sialylated (Sia), and nondecorated (non-Fuc and non-Sia). Data are represented as mean ± SEM ($n = 3$); $^*P < 0.05$; $^{***}P < 0.001$. (*D*) Structures of high-mannose *N*-glycans found in mammalian cells, represented using symbol nomenclature. (*E*) Abundances of extended high-mannose glycan structures (Man 7 to Man 9) in parental and metastatic CCA cells. Data are represented as mean ± SEM ($n = 3$). (*F*) Fold change of glycosylation-related gene expression (normalized to parental) measured by qRT-PCR. Data are represented as mean ± SEM ($n = 3$); $^*P < 0.05$; $^{**}P < 0.01$; $^{***}P < 0.001$. (*G*) Intracellular binding of anti-MAN1A1 in parental and metastatic CCA cells, detected by flow cytometry. FMO, fluorescence minus one.

membrane matrix was up to 3.7-fold ($P < 0.001$) less than the number of uncapped cells (Fig. 3*D*). These results were highly consistent between multiple cell passages (*SI Appendix*, Fig. S5).

While ConA shows specificity to exposed mannose residues, its disadvantages include off-target reactivity and cytotoxicity. Therefore, we used an engineered nonmitogenic lectibody Avaren-Fc (AvFc), which consists of the high-mannose glycan-specific antiviral lectin Avaren fused to the Fc region of human IgG, to block cell surface high-mannose glycan structures with high specificity (30). Under AvFc-bound conditions, migration through micropores diminished 2.2-fold ($P < 0.001$) for KKU-213AL5 and 1.8-fold ($P < 0.01$) for KKU-213BL5 (Fig. 3*E*). Likewise, invasion through the basement membrane matrix diminished 3.2-fold ($P < 0.01$) for KKU-213AL5 and 1.6-fold ($P < 0.05$) for KKU-213BL5 (Fig. 3*F*), an effect consistent with those produced by ConA binding. Collectively, these results

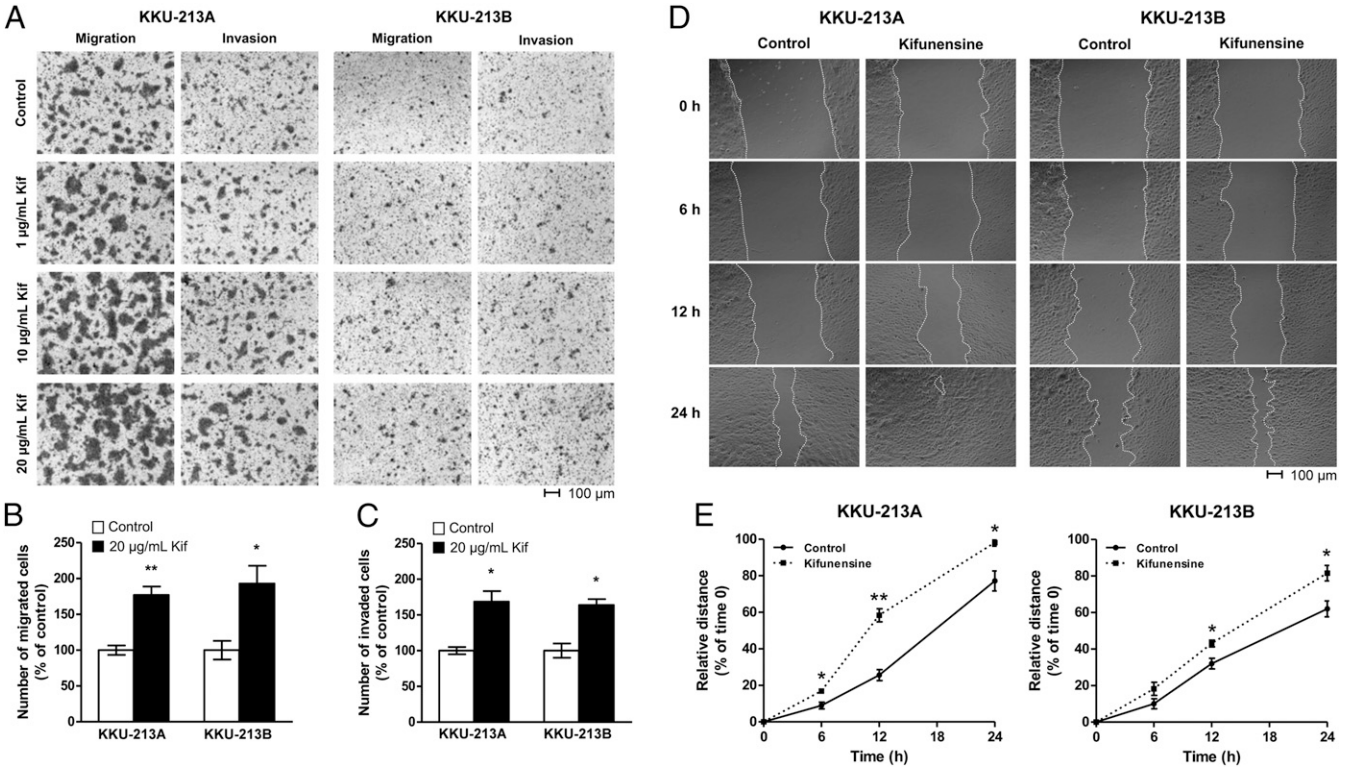

Fig. 2. Enhancement of metastatic phenotypes exhibited by kifunensine-treated parental CCA cells. (*A*) Microscope images of cells that passed through an uncoated (migration) or Matrigel-coated (invasion) microporous polycarbonate membrane under increasing concentrations of kifunensine (Kif). Cells were stained with crystal violet before imaging. (Scale bars, 100 μm.) (*B* and *C*) Number of kifunensine-treated (20 μg/mL) cells that migrated or invaded in comparison to untreated counterparts. Data are represented as mean ± SEM ($n = 3$); $*P < 0.05$; $**P < 0.01$. (*D*) The extent to which a scratch wound was closed by untreated or treated cells over time. (Scale bars, 100 μm.) (*E*) Percentage of closure is presented as a measure that is relative to the distance of the wound at $t = 0$. Data are represented as mean ± SEM ($n = 3$); $*P < 0.05$; $**P < 0.01$.

affirm that high-mannose glycan structures need to be exposed on the surfaces of metastatic CCA cells for migration and invasion.

Overexpression of *MAN1A1* Reduces Tumor Growth. Besides the use of inhibitory mannose-binding proteins, we reduced high-mannose glycosylation by overexpressing *MAN1A1* in metastatic KKU-213AL5 cells, which were more proliferative than KKU-213BL5 cells. Upon transfection with DNA plasmids containing human *MAN1A1* and isolation of stable clones, we consistently observed about 11.7-fold higher expression of *MAN1A1* in *MAN1A1*-transfected cells (hMAN1A1-KKU-213AL5) compared to the control (PBN-KKU-213AL5) (Fig. 3*G*). This transformation resulted in a global decrease in the abundances of extended high-mannose glycans (*SI Appendix*, Fig. S6), which were more readily processed into shorter high-mannose glycans.

Following the generation of *MAN1A1*-overexpressing KKU-213AL5 cells, we evaluated the ability of tumors to form by local s.c. injection into the abdominal flank of NOD-*scid Il2rg*^{null} (NSG) mice. Tumors started to form on day 2 in all mice implanted with PBN-KKU-213AL5 and hMAN1A1-KKU-213AL5, but the rate of growth of hMAN1A1-KKU-213AL5 tumors was significantly lower than that of PBN-KKU-213AL5 tumors (Fig. 3*H*). Tumor volumes at 12 d postinjection of hMAN1A1-KKU-213AL5 were more than 62% smaller than those of PBN-KKU-213AL5 ($P < 0.05$, paired t test). These findings indicate that extended high-mannose glycan expression is associated with the malignant phenotype of CCA.

High-Mannose Glycosylation Sites in CCA Retain Exclusivity against Other Glycoforms. The findings that high-mannose glycosylation may be a contributing factor to the observed phenotypical differences between parental and metastatic CCA prompted examination of the cell surface proteome to determine which proteins display high-mannose glycans. Similar to the glycan profiles, the identities of membrane glycoproteins in parental and metastatic CCA cells showed considerable overlap (Fig. 4*A*). Filtering specifically by glycoforms, we identified a total of 152 nonredundant glycosites associated with 95 membrane proteins on KKU-213A and KKU-213AL5 cells that possessed one or more high-mannose type glycans (Datasets S1–S4). On both cell types, more than 85% of glycosites possessed >Man 6 structures (Fig. 4*B*). Approximately 66% of glycosites on parental and 71% on metastatic CCA cells were homogenously occupied with only high-mannose species in the absence of other *N*-glycan types. Features of the local sequence were examined for predisposition to high-mannose glycan expression (Fig. 4*C* and *SI Appendix*, Fig. S7). Significant differences were observed in the frequency of neutral polar residues, including serine and threonine, in the vicinity of sites with high-mannose exclusivity and sites that possessed high mannose along with other *N*-glycan types. For the latter, neutral polar residues were often located at 3, 8, 9, and 10 amino acid positions upstream of the glycosylation site in KKU-213A and KKU-213AL5 glycoproteins. Common to all high-mannose–bearing glycosylation sites, nonpolar residues, namely leucine and valine, tended to surround the *N*-glycan consensus sequence and positively charged residues, lysine and arginine, were most frequently within 2 to 3 and 5 to 6 positions downstream of the glycosylation site. Cysteine was one of the least frequent residues to be near the consensus sequence.

Whereas only minor differences were observed in the number of high-mannose–bearing proteins, variations in the abundances of select glycoforms were discernible in metastatic and parental CCA cells, which was reflective of the glycomics analysis. Based on the

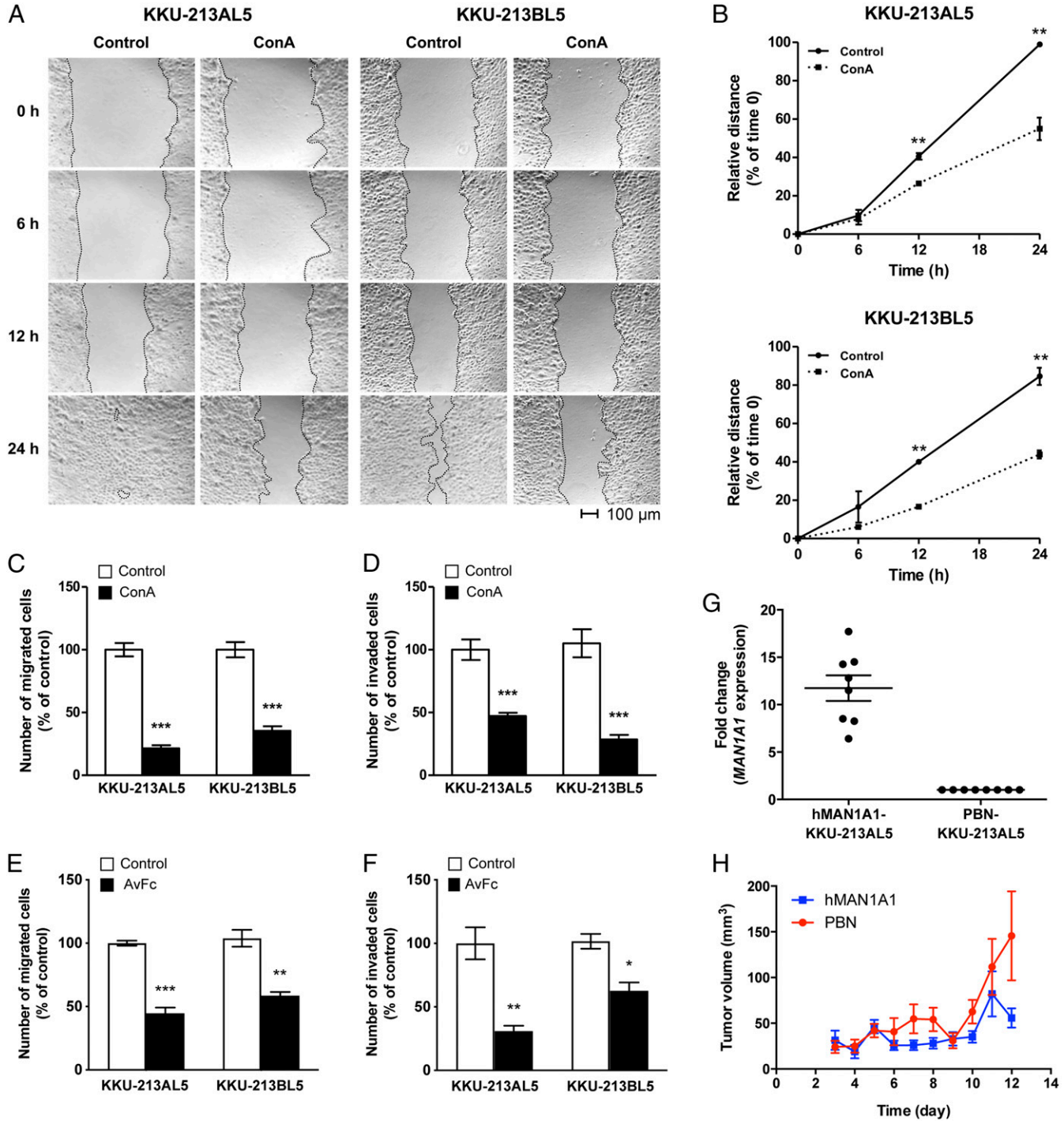

Fig. 3. Reduction of metastatic phenotypes by capping or decreasing high-mannose glycans on metastatic CCA cells. (*A*) The extent to which a scratch wound was closed by untreated or ConA-capped cells over time. (Scale bars, 100 μm.) (*B*) Percentage of closure is presented as a measure that is relative to the distance of the wound at $t = 0$. Data are represented as mean ± SEM ($n = 3$); $^{*}P < 0.05$; $^{**}P < 0.01$. (*C–F*) Enumerated ConA/AvFc-capped cells that passed through an uncoated (migration) or Matrigel-coated (invasion) microporous polycarbonate membrane compared with respect to native cells. Data are represented as mean ± SEM ($n = 3$); $^{*}P < 0.05$; $^{**}P < 0.01$; $^{***}P < 0.001$. (*G*) Quantitative RT-PCR assessment of the increased expression of *MAN1A1* in *MAN1A1*-transfected KKU-213AL5 cells (hMAN1A1-KKU-213AL5) compared to the PBN-transfected control (PBN-KKU-213AL5). Data are represented as mean ± SEM ($n = 6$). (*H*) Volume of tumors formed as a function of time after s.c. injection of PBN- and hMAN1A1-KKU-213AL5 into NSG mice. Data are represented as mean ± SEM ($n = 5$).

sum of the abundances of glycoforms with the same glycan composition, sites occupied with Man 7, Man 8, and Man 9 showed increases of about 25% in metastatic CCA cells relative to parental cells (Fig. 4*D*). In particular, when considering each high-mannose–occupied glycosylation site individually, a fold change of greater than three was observed in 18 unique glycosites on 15 glycoproteins (parental to metastatic; Table 1). This group of glycopeptides was modified with α-1,2-mannose–containing structures,

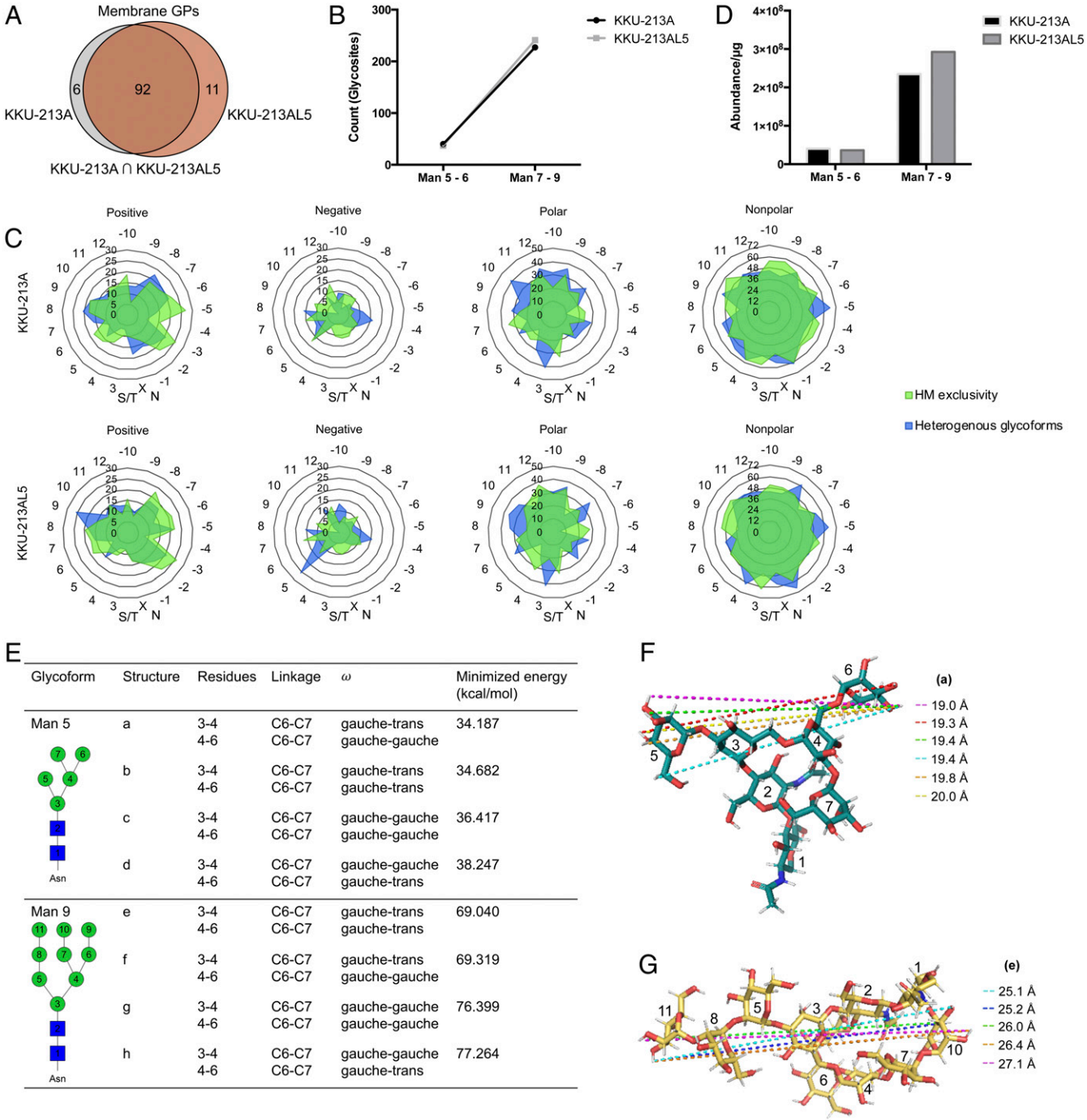

Glycoform	Structure	Residues	Linkage	ω	Minimized energy (kcal/mol)
Man 5	a	3-4 4-6	C6-C7 C6-C7	gauche-trans gauche-gauche	34.187
	b	3-4 4-6	C6-C7 C6-C7	gauche-trans gauche-trans	34.682
	c	3-4 4-6	C6-C7 C6-C7	gauche-gauche gauche-gauche	36.417
	d	3-4 4-6	C6-C7 C6-C7	gauche-gauche gauche-trans	38.247
Man 9	e	3-4 4-6	C6-C7 C6-C7	gauche-trans gauche-trans	69.040
	f	3-4 4-6	C6-C7 C6-C7	gauche-trans gauche-gauche	69.319
	g	3-4 4-6	C6-C7 C6-C7	gauche-gauche gauche-gauche	76.399
	h	3-4 4-6	C6-C7 C6-C7	gauche-gauche gauche-trans	77.264

Fig. 4. Distinction of membrane glycoproteins bearing short and extended high-mannose type *N*-glycans. (*A*) Number of glycosylated proteins (GPs) associated with the membrane of KKU-213A and/or KKU-213AL5 cells. (*B*) Number of glycosylated sites (glycosites) on the membrane proteins of KKU-213A and KKU-213AL5 that bear short (Man 5 to 6) or extended (Man 7 to 9) high-mannose type glycans. (*C*) Frequency of positively charged, negatively charged, polar, and nonpolar amino acid residues surrounding high-mannose–bearing glycosylation sites identified in KKU-213A and KKU-213AL5. Concentric axes show percentage of residues per position relative to the total number of sequons identified in each group. HM, high mannose. Circumferential axes show amino acid position relative to the consensus sequence, N-X-S/T. (*D*) Abundances of high-mannose–bearing glycopeptides as derived from precursor ion peak areas and normalized to the total protein concentration. (*E*) Stable conformations of Man 5 (structures *a*–*d*) and Man 9 (structures *e*–*h*) that arise from conformational isomerism about the C6–C7 bond between residues 3 and 4 and between residues 4 and 6, respectively. (*F* and *G*) The largest spanning distances measured between two atoms in Man 5 (structure *a*) and Man 9 (structure *e*).

Man 6, Man 7, Man 8, and/or Man 9, and showed increases in metastatic CCA cells compared to parental cells. Significantly, upregulated proteins were characterized as being involved in substrate recognition, mediating extracellular interactions, and/or conferring the cell the ability to adhere (*SI Appendix*, Fig. S8).

High-Mannose Glycans Modify Membrane Protein Complex Formation. To reference glycans in relation to the molecular structure of their parent proteins, high-mannose–bearing glycoproteins associated with CCA metastasis were modeled computationally. Man 5 and Man 9 were used to build the model, representing short and

Table 1. Membrane glycoproteins from metastatic KKU-213AL5 cells that exhibited greater than threefold changes in abundance relative to those from parental KKU-213A cells

UniProt accession	Gene name	Protein name	Glycosylation site	Glycan	Fold change*
Q08380	*LGALS3BP*	Galectin-3–binding protein	N551	Man 9	13.67
Q9NYQ6	*CELSR1*	Cadherin EGF LAG seven-pass G-type receptor 1	N1623	Man 9	7.64
Q8IWB1	*ITPRIP*	Inositol 1,4,5-trisphosphate receptor-interacting protein	N27	Man 9	7.20
P11717	*IGF2R*	Cation-independent mannose-6-phosphate receptor	N747	Man 9	7.00
P50895	*BCAM*	Basal cell adhesion molecule	N439	Man 7	6.69
Q08380	*LGALS3BP*	Galectin-3–binding protein	N125	Man 9	6.56
P05556	*ITGB1*	Integrin beta-1	N669	Man 6	5.19
P07942	*LAMB1*	Laminin subunit beta-1	N677	Man 9	4.15
Q8WWI5	*SLC44A1*	Choline transporter-like protein 1	N135	Man 7	4.14
O15230	*LAMA5*	Laminin subunit alpha-5	N95	Man 8	4.12
Q06481	*APLP2*	Amyloid-like protein 2	N541	Man 8	3.88
P02786	*TFRC*	Transferrin receptor protein 1	N727	Man 8	3.84
P78325	*ADAM8*	Disintegrin and metalloproteinase domain-containing protein 8	N91	Man 9	3.83
P06756	*ITGAV*	Integrin alpha-V	N74	Man 7	3.77
Q08380	*LGALS3BP*	Galectin-3–binding protein	N398	Man 7	3.62
Q08380	*LGALS3BP*	Galectin-3–binding protein	N398	Man 8	3.60
P13473	*LAMP2*	Lysosome-associated membrane glycoprotein 2	N356	Man 9	3.48
Q92542	*NCSTN*	Nicastrin	N45	Man 8	3.17
Q08380	*LGALS3BP*	Galectin-3–binding protein	N580	Man 8	3.16
P50895	*BCAM*	Basal cell adhesion molecule	N439	Man 8	3.04

*Parental to metastatic.

extended high-mannose glycan structures, respectively. In solution, different rotameric conformations about the C-C bond at the C6 position of α-1,6–linked sugars give rise to multiple isomers. Considering solely the glycan portion, energy minimization calculations showed that Man 5 and Man 9 adopt one of four stable conformations (Fig. 4*E* and *SI Appendix*, Fig. S9), representing all possible gauche–trans (+60) or gauche–gauche (−60) conformational isomers that occur around residues 3 to 4 and residues 4 to 6 (31). The largest spanning distance between the antennae of Man 9 (isomer *e* or *f*) (27.1 Å) was expectantly greater than that of Man 5 (isomer *a*) (20.0 Å) (Fig. 4 *F* and *G*). In Man 9, this distance extended from the C2 hydroxyl hydrogen of the terminal α2 mannose on the α3 antenna of the α6 arm (residue 10) to the C2 hydroxyl hydrogen of the terminal α2 mannose on the α3 arm (residue 11). In Man 5, the distance ranged from the C5 hydroxyl hydrogen of the terminal α6 mannose on the α6 arm (residue 6) to the C4 hydroxyl hydrogen of the single mannose on the α3 arm (residue 5).

We focused on high-mannose glycosylated membrane proteins that showed prominent changes in CCA metastasis and that have been highlighted as a therapeutic target in other cancers: transferrin receptor protein 1 (TFRC) at Asn-727, integrin alpha-V (ITGAV) at Asn-74, and nicastrin (NCSTN) at Asn-45 (32–34). According to the static, unbound structural conformations, occupied sites were solvent exposed and located on random coils (green residues) near a cavity or pocket within the proteins (blue residues) (Fig. 5*A*), which was suggestive that high-mannose glycans may facilitate interactions with their binding partners. Subsequently, the goodness of each major protein–protein and protein–ligand complex formation was estimated prior to introducing high-mannose glycan variations. As models of the starting nonmannosylated complex, proteins were initially docked to their respective pairs without high-mannose glycans, employing structure refinement with respect to the resolved bound structures. Docked structures showed excellent overlap with experimental structures, as indicated by template modeling score calculations (TM score) and backbone root-mean-square deviations (rmsds) (*SI Appendix*, Fig. S10). Global binding energies were determined from the interaction energies of the docked structures, showing favorable binding of dimerized transferrin receptor protein 1, transferrin receptor protein 1:serotransferrin, integrin αVβ3, integrin αVβ3:RGD peptide, γ-secretase, and γ-secretase:Notch fragment (Fig. 5*B*). In examining the interaction energies, unfavorable repulsive short-range electrostatics interactions were one of the dominant contributions to the binding energy of complexes involving nonmannosylated transferrin receptor protein 1 (Fig. 5*C*). Intriguingly, according to the three-dimensional (3D) representation of the serotransferrin-bound conformation, the glycosylation site of interest was directed away from the ligand-binding sites (Fig. 5*D*). For these reasons, glycosylated transferrin receptor protein 1 was selected for further study to probe the effects of extended high-mannose glycans on the parent protein.

Molecular dynamics simulations were performed with the homodimeric transferrin receptor protein 1 ectodomain bearing high-mannose glycans (Man 5 or Man 9) at residue N727. Backbone rmsds relative to the initial structure indicated that the glycosylated structures were stable over time (*SI Appendix*, Fig. S11). Compared to the aglycosylated protein, the high-mannose glycosylated protein adopted a more "open" conformation, creating space at the dimer interface. The effect was more pronounced with Man 9 than Man 5 glycosylation. Notably, this model suggested that the presence of Man 5 and Man 9 at N727 may lead to displacement of residues in the areas of the receptor that directly bound to the N lobe (N662 to E664) and the C lobe (R629 to R648) of serotransferrin (Fig. 6*A*). According to the electrostatics potential surface, a reduction of the solvent-exposed negative electrostatic contribution was observed in the protease-like domain of Man 5- and Man 9-bearing transferrin receptor protein 1. Conversely, the addition of Man 9 at N727 decreased the positive electrostatic potential on the surface of the apical domain. Electrostatic potential was retained in the serotransferrin-binding domain with either Man 5 or Man 9 glycosylation.

Considering the dimerization of transferrin receptor protein 1, both aglycosylated and high-mannose–glycosylated forms produced exothermic events. As modeled with molecular docking (*SI Appendix*, Fig. S12), aglycosylated protein dimerization was energetically more favorable than high-mannose–glycosylated protein dimerization (Fig. 6*B*). However, contributions from electrostatic repulsion were greatly reduced from 57.7 kcal/mol

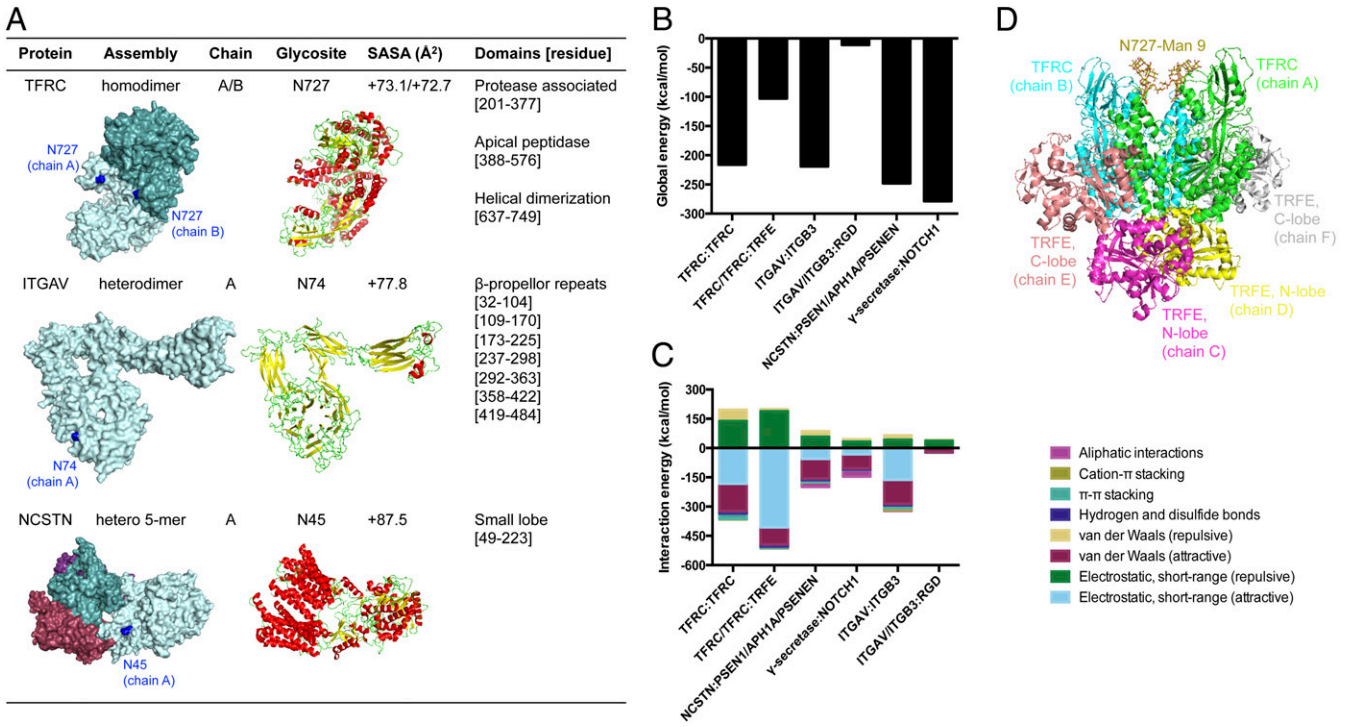

Fig. 5. Localization of high-mannose type glycans within the 3D structures of membrane proteins with elevated abundances in metastatic CCA. (*A*) Surface and cartoon rendition of membrane glycoproteins up-regulated in KKU-213AL5. Protein chains are named alphabetically and distinguished by color. Glycosylated sites of interest are colored in blue. Alpha helices, beta sheets, and coils are colored in red, yellow, and green, respectively. SASA, solvent accessible surface area. (*B*) Global energies of major protein–protein and protein–ligand complexes as determined by molecular docking: transferrin receptor protein 1 (TFRC) homodimer, TFRC:serotransferrin (TRFE), integrin αV (ITGAV):integrin β3 (ITGB3), integrin αVβ3:RGD peptide, γ-secretase (nicastrin [NCSTN]:presenilin-1 [PSEN1]/γ-secretase subunit APH-1A [APH1A]/γ-secretase subunit PEN-2 [PSENEN]), and γ-secretase/Notch-1 fragment (NOTCH1). (*C*) Contributions of interactions to the total energy of complexes. (*D*) An initial 3D model of the TFRC:TRFE complex built by placing Man 9 at the identified site of glycosylation (blue).

in the minimized, equilibrated aglycosylated homodimer system to 19.9 kcal/mol and 6.2 kcal/mol in the Man 5-bearing and Man 9-bearing homodimer assemblies, respectively (Fig. 6 *C–E*). Docked models suggested that hydrogen bonding and disulfide bonding, which play important roles in maintaining the structural architecture of macromolecules, were diminished with high-mannose glycosylation due to the widening at the dimer interface. Intermolecular π–π stacking interactions, which often have a stabilizing effect on protein structures, were conserved in the Man 5-bearing and Man 9-bearing transferrin receptor protein 1 dimer assemblies. In general, having Man 9 at N727 produced a more energetically favorable conformation than with the placement of Man 5. In comparing the aglycosylated and glycosylated ectodomain of transferrin receptor protein 1, it was evident that N727-occupied high-mannose glycoforms induce structural conformational changes that modify charge–charge noncovalent interactions.

Expression of *MAN1A1* and *TFRC* in CCA Tissues. To assess the clinical relevance of high-mannose glycosylation and transferrin receptor protein 1 expression, RNA sequencing data of CCA tissues ($n = 36$) and of matched normal adjacent tissues ($n = 9$) were obtained from The Cancer Genome Atlas (TCGA) research network (Fig. 7*A*) (35). The expression level of *MAN1A1* in tumor tissues was significantly lower than that of matched normal adjacent tissues ($P < 0.001$, Wilcoxon rank-sum test) (Fig. 7*B*). *TFRC* expression was significantly higher in tumor tissues than in normal tissues ($P < 0.001$, Wilcoxon rank-sum test) (Fig. 7*C*). *MAN1A1* expression was positively correlated with that of *TFRC* ($P = 0.015$, Wilcoxon rank-sum test) (Fig. 7*D*). This analysis lends support for the prevalence of high-mannose glycosylation and transferrin receptor protein 1 in CCA.

Discussion

As one of the earliest compounds produced in the *N*-linked glycan biosynthetic pathway, high-mannose type structures constitute a subset of *N*-glycans where the chitobiose core is extended only by mannose residues. Subsequent trimming and transfer of monosaccharides generate more structurally diverse hybrid and complex type *N*-glycans. Interestingly, transformation of a heterogenous arrangement of *N*-glycans on the cell surface to a generally homogenous, uncharged population of extended high-mannose *N*-glycans by kifunensine treatment resulted in accentuation of lateral mobility, transmigration, and invasion of CCA cells. In agreement with this observation, comparative analysis of the glycan profiles between parental and metastatic CCA showed significantly elevated abundances of high-mannose type glycans in the more aggressive cells, KKU-213AL5 and KKU-213BL5. Specifically, isomeric differentiation by LC-MS and qPCR analysis revealed an overabundance of extended high-mannose glycans (Man > 6), arising from lower expression of *MAN1A1*. In turn, overexpression of *MAN1A1* in metastatic CCA cells impaired tumor growth in vivo. Together, these results distinguish extended high-mannose glycans from other *N*-glycans as a major potential contributor of CCA metastasis.

Glycosylation occurs as large, hydrophilic posttranslational modifications of proteins and in this respect plays a critical role in directing higher-order protein structure. Recently, the attachment of fucose to *N*-acetylglucosamine (GlcNAc) at the reducing end of a biantennary complex type *N*-glycan was shown to restrict the conformation of its parent protein, integrin β1, such that the glycan is virtually locked in position (36). Molecular modeling suggested that constraints not only were evident near the core fucose residue but also extended beyond to the antenna.

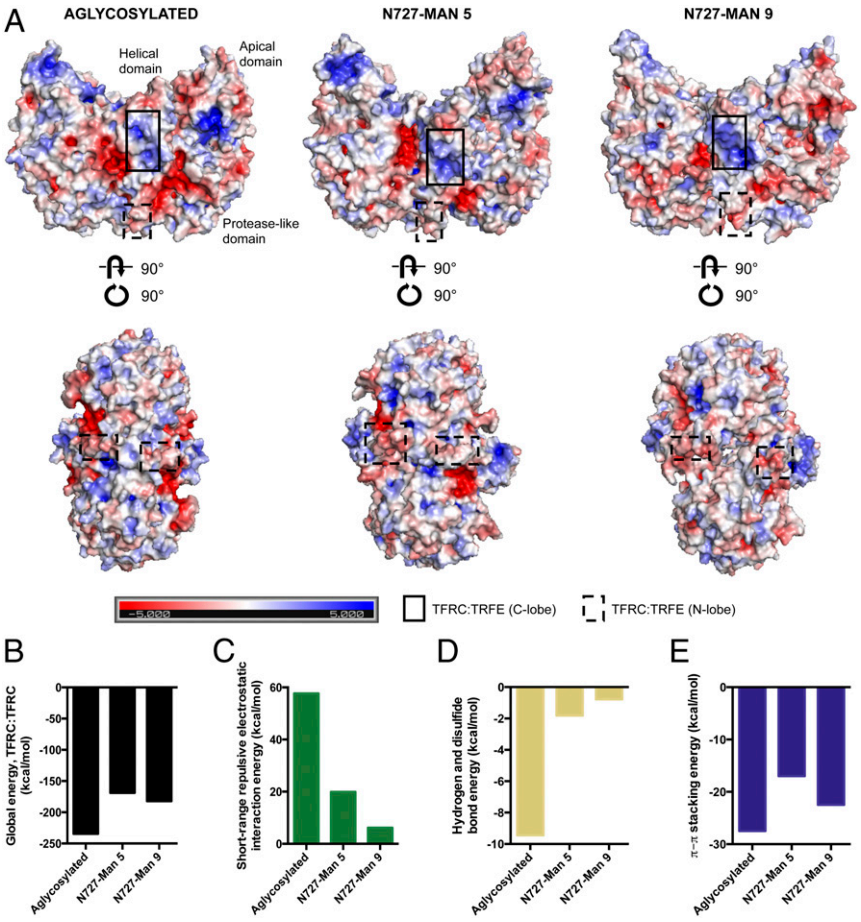

Fig. 6. Dimerization of transferrin receptor protein 1 with and without high-mannose glycosylation. (*A*) Electrostatic potential surfaces of transferrin receptor protein 1 homodimer that bears no glycan, Man 5, or Man 9 at N727 in the minimized, equilibrated system, as calculated with the Adaptive Poisson–Boltzmann Solver (APBS). The color scale mapped on all surfaces ranges from −5 to 5 as shown in the key. Different perspectives of the dimer are depicted in *Top* and *Bottom*. Serotransferrin binding sites are outlined in each perspective. (*B*) Global energies of the aglycosylated, Man 5-bearing, and Man 9-bearing TFRC dimer as determined by molecular docking. (*C*–*E*) Contributions of short-range repulsive electrostatic interactions, hydrogen and disulfide bonds, and π–π stacking to the total energy of the aglycosylated and glycosylated homodimer assemblies.

Extended high-mannose glycan structures possess three antennae with up to 11 total monosaccharides and are covalently linked to the polypeptide skeleton at the reducing end through an asparagine residue, requiring substantial occupancy space and potentially altering the flexibility of the parent proteins to which they are attached. As shown with transferrin receptor protein 1, extended high-mannose glycans can indeed introduce changes to protein conformational dynamics. The homodimer assembly positions the glycans occupying N727 toward one another. Consequently, steric hindrance is likely to accelerate the reorientation of the protein with the addition of extended high-mannose glycans at N727. For the Man 9-glycosylated form, a global effect was observed such that areas near the glycosylation site in addition to areas on the opposite face of the glycosylation site were displaced. While the residue N727 did not directly participate in the binding of serotransferrin, its glycosylation state was critical for shaping the protein conformation and directing ligand affinity as a result, with Man 9 producing a more favorable orientation than Man 5. The dependence of glycans at N727 for transferrin receptor protein 1 folding and function has been supported by site-directed mutagenesis (37). Of note, high iron accumulation has been shown to be strongly correlated with poor prognosis of patients with CCA (38). Collectively, the data suggest that increased abundance of Man 9-bearing transferrin receptor protein 1 produces less repulsion at the dimer interface to support dimerization and promote movements that facilitate serotransferrin binding, increasing iron uptake. In turn, iron excess may play a role in stimulating cell migration through TNF-induced signaling or production of reactive oxygen species (39, 40). Following iron release, transferrin receptor protein 1 is recycled back to the cell surface. It has been proposed that a redistribution to the leading edge of lamellae in a polarized fashion helps cells translocate (41). High-mannose glycosylation, which is correlated with high turnover rates (42), may also be involved in stabilizing the return of transferrin receptor protein 1 to the cell surface. Elevated intracellular iron levels and augmented rates of transferrin receptor protein 1 recycling may link increased Man 9 production to CCA cells acquiring metastatic phenotypes.

The main route of metastatic spread involves endothelial transmigration, which requires rapid and reversible changes to membrane assembly. Importantly, membrane proteins are richly modified with glycan structures that readily exhibit changes with disruptions of homeostasis. Earlier studies affirm that while glycans regulate the catalytic activity of certain proteins, others may not be affected by glycosylation changes (29, 43). The ability to trace glycans to their parent proteins is necessary to interpret how alterations in glycan expression patterns lead to enhancement of metastatic phenotypes but is lacking in earlier studies (44). Our approach evaluated extended high-mannose glycans

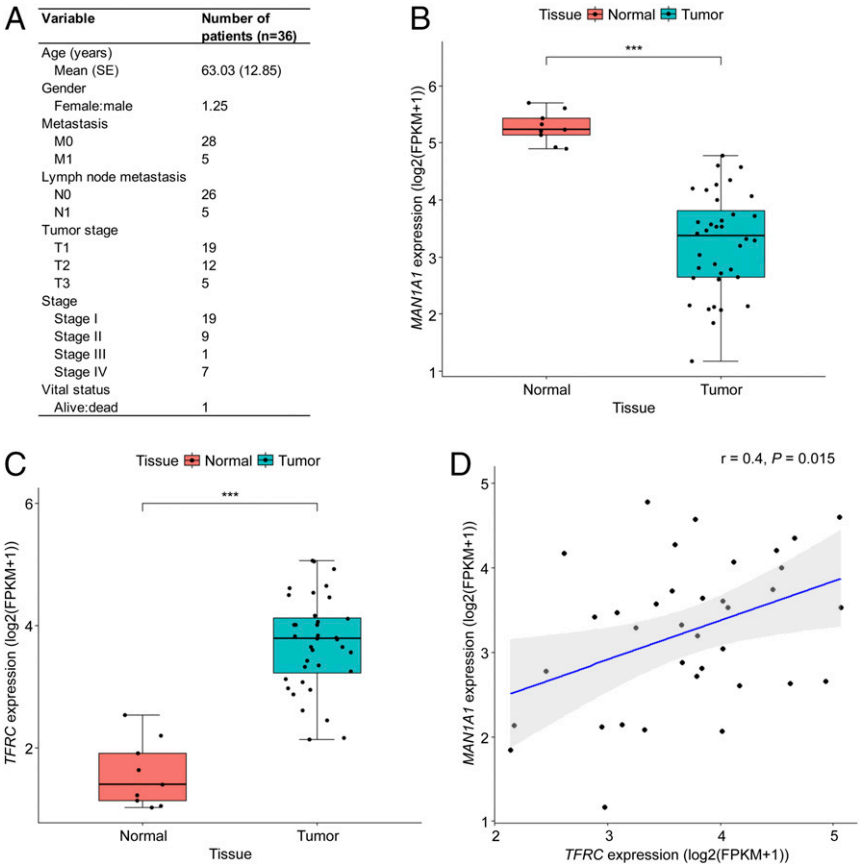

Fig. 7. Expression of *MAN1A1* and *TFRC* in human CCA tissues. (*A*) Clinical characteristics of patients with primary tumor in the TCGA-CHOL cohort. (*B* and *C*) Box plots of *MAN1A1* and *TFRC* expression in CCA tissues ($n = 36$) and matched normal adjacent tissues ($n = 9$). FPKM, fragments per kilobase million; ***$P <$ 0.001. (*D*) Correlation scatter plot of *MAN1A1* and *TFRC* expression in normal and CCA tissues. *r*, Pearson correlation coefficient.

together with their parent glycoproteins. From this analysis, a target group of α-1,2–mannsosylated glycoprotein candidates in addition to glycosylation sites that are likely to play a role in CCA progression were identified. Furthermore, quantification of site-specific differences enabled discovery of specific glycoforms that were differentially regulated on the cell surface of metastatic CCA. A number of the up-regulated high-mannose–containing glycoproteins we identified have been previously implicated in solid tumor metastasis, including integrin αV, integrin β1, cadherin family member 9, galectin-3–binding protein, basal cell adhesion molecule, and disintegrin and metalloproteinase domain-containing protein 8 (45–49). Nonetheless, the connection between their glycosylation and tumor aggression remains underdeveloped. Our studies show that 1) the majority of CCA proteins bear extended high-mannose glycans; 2) the abundances of glycoforms containing short high-mannose glycan structures with five or six mannose residues remain unaltered in highly metastatic CCA compared to parental tumor cells; 3) high-mannose glycan expression can lead to reductions in the dynamic freedom of receptor proteins and modulate substrate binding based on the position of glycosylation; and 4) whereas certain high-mannose–containing sites accommodate other glycan types, many retain exclusivity to high-mannose structures. The observed patterns of extended high-mannose glycosylation within membrane proteins suggest that there is a certain local environment that prevents further processing arising from lack of accessibility by α-mannosidases.

This work constitutes a comprehensive catalog of cell surface oligosaccharide compositions that correlate with metastatic transformation, providing a guide for molecular studies to probe the participation of altered glycans in CCA metastasis. We demonstrate that a shift toward α-1,2-mannosylation arising from the decrease in expression of MAN1A1 can provide structural rigidity to underlying proteins due in part to the location of the relevant glycosylation site. A unique advantage may be conferred to metastatic CCA cells with dominance of extended high-mannose glycosylation by priming extracellular receptors for ligand recruitment and binding. Future studies are warranted to examine whether other cancer types with elevated levels of high-mannose type glycans, including breast and colorectal adenocarcinomas, follow a similar mode of spread that is supported by extended high-mannose glycosylation. Given the heterogenous nature of cell glycosylation, other glycan types that were differentially expressed in metastatic CCA including sialylated and/or fucosylated *N*-glycans may also play a role in the progression of CCA. We postulate that understanding the density of glycan molecules and their parent proteins on metastatic CCA and differentiating the silent from actionable targets will aid in the development of additional classes of selective glycan-based molecular probes.

Materials and Methods

Details of the experimental protocols can be found in *SI Appendix*.

Wound Healing Assay. KKU-213A, KKU-213AL5, KKU-213B, and KKU-213BL5 (50,000 cells per well) were seeded into 24-well plates in serum-free media and allowed to grow until a monolayer was formed. A single scratch wound was applied to every well before incubation at 37 °C. Images were captured after 6, 12, and 24 h on a Leica DMI3000B microscope (Leica Microsystems). Four replicates were prepared for each treatment group.

Migration and Invasion Assay. Porous filter polycarbonate membrane inserts (8 μm; Corning) were placed into individual wells on a 24-well plate, creating two separate chambers. After harvest with trypsin/EDTA, 40,000 cells were added in serum-free media to the top chamber while the bottom chamber was filled with complete media. For the invasion assay, the inserts were coated with 100 μL of 0.4 mg/mL Matrigel basement membrane matrix (Corning) in serum-free media overnight at 37 °C, which was subsequently removed prior to seeding cells. After 9 h (KKU-213A, KKU-213AL5) or 24 h (KKU-213B, KKU-213BL5), cells that transferred through the pores were fixed with 4% (vol/vol) paraformaldehyde, stained with 0.5% (wt/vol) crystal violet, washed, and imaged on a Leica DMI3000B microscope (Leica Microsystems). Per insert, the number of cells was counted from five microscopic fields of view captured with a 10× objective. Four replicates were prepared for each treatment group.

Mouse Model for Tumor Growth. All animal studies were conducted according to a University of California, Davis Institutional Animal Care and Use Committee (IACUC)-approved protocol. Five-week-old female NSG mice were purchased from Jackson Laboratory. Each mouse was s.c. injected with 1.5×10^6 KKU-213AL5 cells transfected with the empty vector (PBN) and 1.5×10^6 KKU-213AL5 cells transfected with human *MAN1A1* (hMAN1A1) in 200 μL of PBS into the left or right side of the shaved abdominal flank, respectively, in the supine position. Mice were monitored daily upon formation of tumors between day 3 and day 12. Tumors were measured using a caliper and tumor volume was calculated as $V = (\text{length} \times \text{width}^2)/2$. According to the protocol, mice were euthanized when exhibiting signs of discomfort.

Cell Membrane Glycomics and Glycoproteomics. Extraction of cell membrane proteins and LC-MS/MS analyses were performed as described previously (50, 51).

Molecular Docking. Proteins that were up-regulated in CCA metastasis were used to perform a model-based docking protocol using FireDock (52). The following complexes were accessed from the Protein Data Bank (PDB) for refinement: transferrin receptor protein 1 (1CX8); transferrin receptor protein 1:serotransferrin (1SUV), integrin αVβ3 (1JV2), integrin αVβ3:Arg-Gly-Asp (1L5G), γ-secretase (5FN3), and γ-secretase:Notch 1 (6IDF). Docking solutions were evaluated by alignment with the PDB structures using the TM score (53). Binding energies of the solutions were determined using FireDock.

Data Availability. The data discussed in this paper are available upon reasonable request.

ACKNOWLEDGMENTS. We thank Anthony Herren at the University of California, Davis (UC Davis) Proteomics Core for assistance with Orbitrap performance and the Extreme Science and Engineering Discovery Environment (XSEDE) for computing resources. XSEDE is supported by National Science Foundation Grant ACI-1548562. The results shown here are in part based upon data generated by the TCGA research network: https://www.cancer.gov/about-nci/organization/ccg/research/structural-genomics/tcga. This work was supported by the National Institutes of Health under Awards R01GM049077 (to C.B.L.) and DP2OD008752 (to E.M.) and by the Post-Doctoral Training Program by Research Affairs and Graduate School at Khon Kaen University under Award 59151 (to C.P. and S.W.). This work was also supported by the UC Davis Immune Monitoring Shared Resource under Award 5P30CA093373.

1. T. Bogenrieder, M. Herlyn, Axis of evil: Molecular mechanisms of cancer metastasis. *Oncogene* **22**, 6524–6536 (2003).
2. P. Friedl, K. Wolf, Tumour-cell invasion and migration: Diversity and escape mechanisms. *Nat. Rev. Cancer* **3**, 362–374 (2003).
3. T. R. Geiger, D. S. Peeper, Metastasis mechanisms. *Biochim. Biophys. Acta* **1796**, 293–308 (2009).
4. S. A. Khan, H. C. Thomas, B. R. Davidson, S. D. Taylor-Robinson, Cholangiocarcinoma. *Lancet* **366**, 1303–1314 (2005).
5. D. H. Dube, C. R. Bertozzi, Glycans in cancer and inflammation'–potential for therapeutics and diagnostics. *Nat. Rev. Drug Discov.* **4**, 477–488 (2005).
6. M. J. Kailemia, D. Park, C. B. Lebrilla, Glycans and glycoproteins as specific biomarkers for cancer. *Anal. Bioanal. Chem.* **409**, 395–410 (2017).
7. C. A. Reis, H. Osorio, L. Silva, C. Gomes, L. David, Alterations in glycosylation as biomarkers for cancer detection. *J. Clin. Pathol.* **63**, 322–329 (2010).
8. S. R. Stowell, T. Ju, R. D. Cummings, Protein glycosylation in cancer. *Annu. Rev. Pathol.* **10**, 473–510 (2015).
9. J. W. Dennis, M. Granovsky, C. E. Warren, Protein glycosylation in development and disease. *BioEssays* **21**, 412–421 (1999).
10. E. Maverakis *et al.*, Glycans in the immune system and the altered glycan theory of autoimmunity: A critical review. *J. Autoimmun.* **57**, 1–13 (2015).
11. V. Engelstaedter *et al.*, Expression of the carbohydrate tumour marker Sialyl Lewis A, Sialyl Lewis X, Lewis Y and Thomsen-Friedenreich antigen in normal squamous epithelium of the uterine cervix, cervical dysplasia and cervical cancer. *Histol. Histopathol.* **27**, 507–514 (2012).
12. T. Nakagoe *et al.*, Increased expression of sialyl Lewis(x) antigen as a prognostic factor in patients with stage 0, I, and II gastric cancer. *Cancer Lett.* **175**, 213–221 (2002).
13. H. Satoh *et al.*, Elevated serum sialyl Lewis X-i antigen levels in non-small cell lung cancer with lung metastasis. *Respiration* **65**, 295–298 (1998).
14. S. H. Itzkowitz *et al.*, Expression of Tn, sialosyl-Tn, and T antigens in human colon cancer. *Cancer Res.* **49**, 197–204 (1989).
15. M. A. Carrascal *et al.*, Sialyl Tn-expressing bladder cancer cells induce a tolerogenic phenotype in innate and adaptive immune cells. *Mol. Oncol.* **8**, 753–765 (2014).
16. M. Granovsky *et al.*, Suppression of tumor growth and metastasis in Mgat5-deficient mice. *Nat. Med.* **6**, 306–312 (2000).
17. M. L. A. de Leoz *et al.*, Glycomic approach for potential biomarkers on prostate cancer: Profiling of N-linked glycans in human sera and pRNS cell lines. *Dis. Markers* **25**, 243–258 (2008).
18. M. L. A. de Leoz *et al.*, High-mannose glycans are elevated during breast cancer progression. *Mol. Cell. Proteomics* **10**, M110.002717 (2011).
19. Z. Kyselova *et al.*, Alterations in the serum glycome due to metastatic prostate cancer. *J. Proteome Res.* **6**, 1822–1832 (2007).
20. R. Kannagi, M. Izawa, T. Koike, K. Miyazaki, N. Kimura, Carbohydrate-mediated cell adhesion in cancer metastasis and angiogenesis. *Cancer Sci.* **95**, 377–384 (2004).
21. R. Kleene, M. Schachner, Glycans and neural cell interactions. *Nat. Rev. Neurosci.* **5**, 195–208 (2004).
22. Y. van Kooyk, G. A. Rabinovich, Protein-glycan interactions in the control of innate and adaptive immune responses. *Nat. Immunol.* **9**, 593–601 (2008).
23. L. V. Hooper, J. I. Gordon, Glycans as legislators of host-microbial interactions: Spanning the spectrum from symbiosis to pathogenicity. *Glycobiology* **11**, 1R–10R (2001).
24. X. Huang *et al.*, Glycosylation affects both the three-dimensional structure and antibody binding properties of the HIV-1IIIB GP120 peptide RP135. *Biochemistry* **36**, 10846–10856 (1997).
25. M. J. Feige *et al.*, Structure of the murine unglycosylated IgG1 Fc fragment. *J. Mol. Biol.* **391**, 599–608 (2009).
26. K. Uthaisar *et al.*, Establishment and characterization of a novel human cholangiocarcinoma cell line with high metastatic activity. *Oncol. Rep.* **36**, 1435–1446 (2016).
27. C. Phoomak *et al.*, O-GlcNAcylation mediates metastasis of cholangiocarcinoma through FOXO3 and MAN1A1. *Oncogene* **37**, 5648–5665 (2018).
28. D. Park *et al.*, Salmonella Typhimurium enzymatically landscapes the host intestinal epithelial cell surface glycome to increase invasion. *Mol. Cell. Proteomics* **15**, 3653–3664 (2016).
29. D. Park *et al.*, Enterocyte glycosylation is responsive to changes in extracellular conditions: Implications for membrane functions. *Glycobiology* **27**, 847–860 (2017).
30. K. T. Hamorsky *et al.*, Engineering of a lectibody targeting high-mannose-type glycans of the HIV envelope. *Mol. Ther.* **27**, 2038–2052 (2019).
31. R. J. Woods, Predicting the structures of glycans, glycoproteins, and their complexes. *Chem. Rev.* **118**, 8005–8024 (2018).
32. E. Ryschich *et al.*, Transferrin receptor is a marker of malignant phenotype in human pancreatic cancer and in neuroendocrine carcinoma of the pancreas. *Eur. J. Cancer* **40**, 1418–1422 (2004).
33. J. S. Desgrosellier, D. A. Cheresh, Integrins in cancer: Biological implications and therapeutic opportunities. *Nat. Rev. Cancer* **10**, 9–22 (2010).
34. Y. Lombardo *et al.*, Nicastrin regulates breast cancer stem cell properties and tumor growth in vitro and in vivo. *Proc. Natl. Acad. Sci. U.S.A.* **109**, 16558–16563 (2012).
35. J. N. Weinstein *et al.*; Cancer Genome Atlas Research Network, The Cancer Genome Atlas pan-cancer analysis project. *Nat. Genet.* **45**, 1113–1120 (2013).
36. B. Awan *et al.*, FGF2 induces migration of human bone marrow stromal cells by increasing core fucosylations on N-glycans of integrins. *Stem Cell Reports* **11**, 325–333 (2018).
37. A. M. Williams, C. A. Enns, A mutated transferrin receptor lacking asparagine-linked glycosylation sites shows reduced functionality and an association with binding immunoglobulin protein. *J. Biol. Chem.* **266**, 17648–17654 (1991).
38. W. Jamnongkan *et al.*, Upregulation of transferrin receptor-1 induces cholangiocarcinoma progression via induction of labile iron pool. *Tumour Biol.* **39**, 1010428317717655 (2017).
39. K. A. Ishii *et al.*, Coordination of PGC-1β and iron uptake in mitochondrial biogenesis and osteoclast activation. *Nat. Med.* **15**, 259–266 (2009).
40. P. Liu *et al.*, Deferoxamine-induced increase in the intracellular iron levels in highly aggressive breast cancer cells leads to increased cell migration by enhancing TNF-α-dependent NF-κB signaling and TGF-β signaling. *J. Inorg. Biochem.* **160**, 40–48 (2016).
41. M. S. Bretscher, Cells can use their transferrin receptors for locomotion. *EMBO J.* **11**, 383–389 (1992).
42. G. Xu *et al.*, Unveiling the metabolic fate of monosaccharides in cell membranes with glycomic and glycoproteomic analyses. *Chem. Sci. (Camb.)* **10**, 6992–7002 (2019).

43. H. Xiao, J. M. Smeekens, R. Wu, Quantification of tunicamycin-induced protein expression and N-glycosylation changes in yeast. *Analyst* **141**, 3737–3745 (2016).
44. K. Talabnin, C. Talabnin, M. Ishihara, P. Azadi, Increased expression of the high-mannose *M6N2* and *NeuAc3H3N3M3N2F* tri-antennary *N*-glycans in cholangiocarcinoma. *Oncol. Lett.* **15**, 1030–1036 (2018).
45. A. Stachurska, J. Elbanowski, H. M. Kowalczyńska, Role of $\alpha5\beta1$ and $\alpha v\beta3$ integrins in relation to adhesion and spreading dynamics of prostate cancer cells interacting with fibronectin under in vitro conditions. *Cell Biol. Int.* **36**, 883–892 (2012).
46. S. Yano, S. Kakiuchi, H. Zhang, S. Sone, "Organotropism of lung cancer metastasis and its molecular targeted therapy" in *Integration/Interaction of Oncologic Growth*, G. G. Meadows, Ed. (Springer, Dordrecht, The Netherlands, 2005), pp. 387–405.
47. E. Piccolo *et al*., LGALS3BP, lectin galactoside-binding soluble 3 binding protein, induces vascular endothelial growth factor in human breast cancer cells and promotes angiogenesis. *J. Mol. Med. (Berl.)* **91**, 83–94 (2013).
48. A. Bartolini *et al*., BCAM and LAMA5 mediate the recognition between tumor cells and the endothelium in the metastatic spreading of KRAS-mutant colorectal cancer. *Clin. Cancer Res.* **22**, 4923–4933 (2016).
49. M. Romagnoli *et al*., ADAM8 expression in invasive breast cancer promotes tumor dissemination and metastasis. *EMBO Mol. Med.* **6**, 278–294 (2014).
50. D. Park *et al*., Characteristic changes in cell surface glycosylation accompany intestinal epithelial cell (IEC) differentiation: High mannose structures dominate the cell surface glycome of undifferentiated enterocytes. *Mol. Cell. Proteomics* **14**, 2910–2921 (2015).
51. D. D. Park *et al*., Membrane glycomics reveal heterogeneity and quantitative distribution of cell surface sialylation. *Chem. Sci.* **9**, 6271–6285 (2018).
52. E. Mashiach, D. Schneidman-Duhovny, N. Andrusier, R. Nussinov, H. J. Wolfson, FireDock: A web server for fast interaction refinement in molecular docking. *Nucleic Acids Res.* **36**, W229-32 (2008).
53. Y. Zhang, J. Skolnick, Scoring function for automated assessment of protein structure template quality. *Proteins* **57**, 702–710 (2004).